JOURNAL OF MATERIALS SCIENCE 19 (1984) 785–793

Electrical conductivity/microstructural relationships in aged CaO and CaO + MgO partially-stabilized zirconia

N. BONANOS, R. K. SLOTWINSKI, B. C. H. STEELE, E. P. BUTLER
Wolfson Unit for Solid State Ionics, Department of Metallurgy and Materials Science, Imperial College of Science and Technology, London SW7, UK

Samples of CaO and CaO + MgO partially-stabilized zirconia (PSZ), solution treated at 1830° C and aged at 1400° C to produce a fine dispersion of tetragonal precipitates, were subjected to a.c. electrical measurements in the frequency range 10^{-3} to 10^{6} Hz, at a temperature of 300° C. The component of resistivity due to the grain interiors, obtained from plots of complex resistivity, showed three stages of behaviour, attributed to equilibration, coarsening and finally transformation of a tetragonal precipitate into a more resistive monoclinic phase. A model of the electrical response of a dispersion of particles was used to estimate the conductivities of the constituent phases of the PSZ ceramic and to simulate the complex resistivity data obtained.

1. Introduction

Pure zirconia exists in three polymorphic forms: the cubic fluorite-type phase (c) stable above 2370° C, the tetragonal phase (t) stable between 1170 and 2370° C and the monoclinic phase (m) stable below 1170° C. Pure zirconia cannot be fabricated as a ceramic because the t → m transformation is accompanied by a disruptive 3.5% decrease in volume [1]. For this reason ceramic "alloys" based on zirconia have been developed which contain additions of certain oxides to retain the cubic phase at lower temperatures, for example Y_2O_3 (8 to 9 mol%), CaO or MgO (12 to 13 mol%). The aliovalent ions substitute for zirconium ions in the cubic phase and oxygen vacancies are introduced by charge compensation. At high temperatures (above ≃ 700° C) such fully-stabilized materials are good ionic conductors and find application as electrolytes in oxygen monitors and other electrochemical devices [2, 3]. Their mechanical properties, however, are quite poor. Ceramics with a lower concentration of stabilizer, partially-stabilized zirconias (PSZ), normally consist of a dispersion of tetragonal particles in a cubic matrix. Such materials have useful mechanical strength, fracture toughness and thermal shock resistance, but at high temperatures generally display a lower electrical conductivity than fully-stabilized zirconia [4, 5]. Work on CaO–PSZ [1, 6–8], MgO–PSZ [8–11], and Y_2O_3–PSZ [12] has shown that the mechanical properties can be optimized by heat treatment. This consists of an initial excursion into the single-phase cubic solid solution region of the phase, followed by cooling, in which tetragonal precipitates nucleate homogeneously. Subsequent ageing (typically at 1400° C) in the c + t region, equilibrates the composition of the t precipitates and causes them to coarsen. For particles below a certain critical size (typically ≃ 100 nm) the t → m transformation can be induced by a stress field, such as that associated with a propagating crack. This gives rise to a stress relief mechanism known as transformation toughening [13]. Particles above the critical size, however, will transform spontaneously on cooling to room temperature. Hence overageing produces a c matrix with m particles, possessing inferior mechanical properties. Since the c, t and m phases will not, in general, have identical electrical properties, the microstructural changes on heat treatment should, in prin-

0022–2461/84 $03.00 + .12

ciple, affect the electrical properties of PSZ. This suggests that electrical measurements might provide useful information about ageing and the t → m transformation sequence.

The aim of this work was to measure the a.c. electrical properties of PSZ after ageing and to relate these to microstructural changes as deduced from X-ray diffraction and transmission electron microscopic (TEM) studies. In a previous investigation [14] we have qualitatively explored the effect of ageing on the electrical conductivity of CaO–PSZ. In this contribution a quantitative interpretation is made, based on the use of mathematical models for the conductivity of two-phase mixtures. As an initial step, therefore, the background to this theory will be examined.

2. Theoretical modelling

Bauerle [15] first showed that the a.c. response of a polycrystalline sample of zirconia contains contributions from the grain interiors, the grain boundaries and the electrolyte/electrode interface, and can be represented by a simple circuit in which the three components are connected in series (Fig. 1a). This circuit bears a direct relationship to the complex impedance plot (Fig. 1b) in which Z'', the imaginary part of the complex conjugate of impedance, is plotted against Z', the real part, for a number of frequencies. The resistances R_{gi}, R_{gb} and R_e, corresponding to grain interior, grain boundary and electrode respectively, may be estimated from the diameters of the semicircles in this plot. In practice, experimental impedance plots consist of arcs, the chord lengths of which give the resistances. The corresponding capacitances of the three components may be calculated from frequencies f_{gi}, f_{gb}, and f_e, shown in Fig. 1b, using the formula $C = (2\pi fR)^{-1}$. These frequencies may be read from plots of Z' against $\log f$, in which they correspond to $Z'(f_{gi}) = \frac{1}{2}R_{gi}$, $Z'(f_{gb}) = R_{gi} + \frac{1}{2}R_{gb}$, etc. If the arcs are not perfect semicircles, however, the capacitances obtained by this method will be approximate.

Since PSZ has a two-phase microstructure, it is necessary to consider models for the a.c. electrical properties of two-phase dispersions [16, 17]. A model presented by Fricke [18, 19] treats the electrical properties of a random dispersion of ellipsoidal particles in a continuous medium. The results are expressed in terms of complex conductivity ψ, defined by:

$$\psi = \sigma + j\omega\epsilon \qquad (1)$$

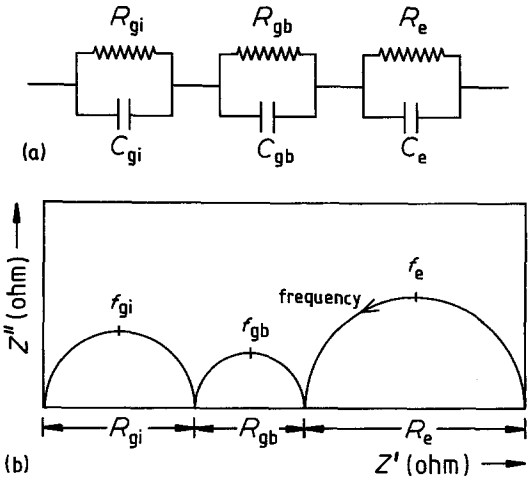

Figure 1 (a) Equivalent circuit for the electrical response of a polycrystalline sample of zirconia, showing contributions from the grain interiors (gi), grain boundaries (gb) and electrolyte/electrode interface (e). (b) Complex impedance plot corresponding to the circuit in Fig. 1a.

where σ is the conductivity, ϵ is the absolute permittivity and ω is the angular frequency of the alternating electric field. The complex conductivity equation derived is:

$$\psi_0 = \psi_2 + \frac{(\psi_1 - \psi_2)(1 - x_2)}{1 + \frac{x_2}{3}\sum_{n=1}^{3}\frac{\psi_1 - \psi_2}{\phi_n\psi_1 + \psi_2}} \qquad (2)$$

where ψ_0 is the complex conductivity of the dispersion,

ψ_1, ψ_2 are the complex conductivities of the matrix and the dispersed phase respectively,

x_2 is the volume fraction of the dispersed phase, and

$\phi_{1,2,3}$ are form factors which depend on the axial ratios of the ellipsoidal particles defined by the semiaxes a, b, c, where $a \geqslant b \geqslant c$.

The range of the volume fraction x_2 of the dispersed phase over which this equation is valid has never been accurately specified, but is believed to be from 0 to 0.3. At higher volume fractions, the electric fields around the particles are expected to interact and the model should be less accurate. In addition, the second phase particles would eventually connect at high volume fractions to form continuous paths, thus invalidating the model. The degree of connectivity would depend on the shape and orientation of the particles.

For very dilute dispersions ($x_2 \simeq 1\%$) the elec-

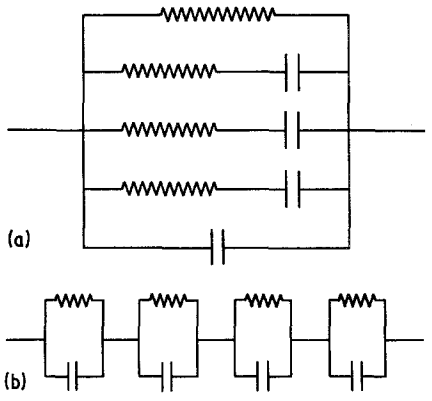

Figure 2 (a) Parallel equivalent circuit for the electrical response of a two-phase random dispersion of ellipsoidal particles [19]. (b) Series-connected equivalent of circuit in Fig. 2a.

trical response is identical to that of a homogeneous suspension of ellipsoids aligned along the three principal orientations [19]. This result is relevant to the present work because the PSZ samples consist of randomly oriented grains, with each grain containing oriented precipitates [20]. The dispersion can be represented by the circuit shown in Fig. 2a [19], or its electrical equivalent shown in Fig. 2b, consisting of four series-connected R–C elements, each of which has its own time constant [21]. For ellipsoids of higher symmetry (spheroids, spheres) the number of elements decreases, so that for spheres, where orientation is immaterial, Equation 2 reduces to the well known Maxwell–Wagner model [22, 23].

Meredith and Tobias [17] have used the low volume fraction approximation of Fricke's model as a basis for more elaborate models for higher volume fractions. These models, however, are only valid for d.c. conductivity, and have not, therefore, been used here.

3. Experimental procedure

The ceramics used in this investigation were compositions prepared by Anderman & Ryder Ltd; details of the preparation have been given elsewhere [14]. The compositions of the materials were 8.0 mol% CaO in CaO–PSZ and 6.6 mol% CaO with 3.2 mol% MgO in CaO + MgO–PSZ. They were chosen to minimize the solution treatment temperature while providing a high volume fraction of the tetragonal phase. In the ternary composition the CaO/MgO ratio was additionally chosen to reduce the t coherency strains. Solution treatment was carried out in the single-phase cubic field, in air at 1830° C for 3 h, and was followed by a furnace cool to room temperature. Subsequent ageing was performed at 1400° C for both compositions. During heat treatment the samples were surrounded with powder of the same composition to prevent loss of stabilizer.

X-ray diffraction was carried out using a powder diffractometer with a rotating sample holder, on samples polished to 1 μm diamond. For a volume fraction determination, the intensities of $(1\,1\,1)_m$, $(1\,1\,\bar{1})_m$ and $(1\,1\,1)_c$ peaks were determined in CaO–PSZ overaged for 30 h, in which the tetragonal phase could no longer be observed. This method was not applied to the CaO + MgO–PSZ samples because the t → m transformation following ageing, proceeds to completion over a far greater ageing time range [14]. The tetragonal precipitate content of the underaged and peak aged CaO–PSZ was taken to be equal to the monoclinic phase content of the overaged material. This approximation is considered to be valid since the t → m transformation is martensitic, and the volume fraction of grain boundary monoclinic phase is very low. The formula used to calculate the monoclinic volume fraction [24] was

$$x_m = \frac{I(1\,1\,1)_m + I(1\,1\,\bar{1})_m}{I(1\,1\,1)_m + I(1\,1\,\bar{1})_m + I(1\,1\,1)_c}. \quad (3)$$

The samples used for X-ray diffraction were also used for a.c. impedance measurements. After solvent cleaning, they were baked out at 400° C for 10 min and their faces sputtered with a continuous layer of platinum. Impedance measurements were performed in a temperature-controlled furnace with screened leads extending to within 1 cm of the sample. With this precaution the stray capacitance across the sample was kept below 0.5 pF and electrical noise was minimal. The measurement system was based on a microcomputer-controlled Solatron 1174 frequency response analyser. The results were presented in terms of the complex resistivity ρ^*, which is defined as

$$\rho^* = Z^* A/d, \quad (4)$$

where Z is the complex impedance, A the cross-sectional area and d the thickness of the sample. Impedance measurements were conducted over the frequency range 10^{-3} to 10^6 Hz, with an applied potential of 0.2 V, at a temperature of 300° C. At this temperature the frequency response of our equipment covered the grain interior and the grain

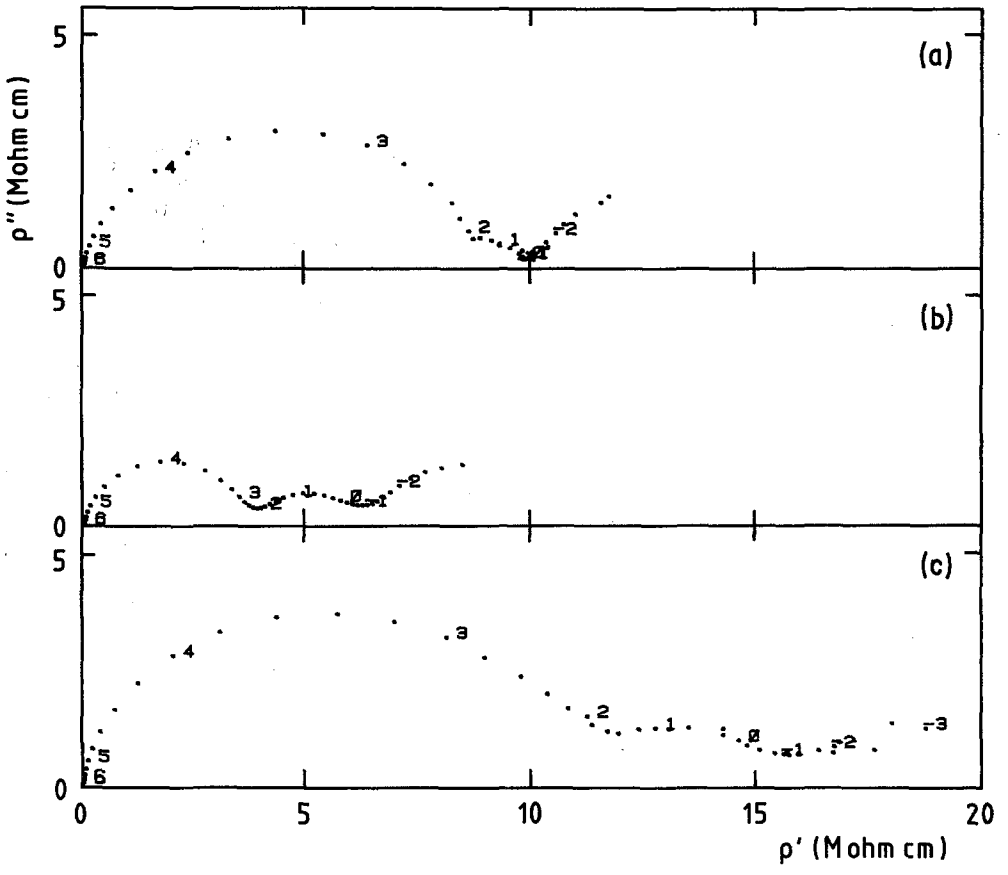

Figure 3 Complex resistivity plots obtained at 300° C for CaO–PSZ samples: (a) as-fired, (b) aged 15 h, (c) aged 30 h. Numbers on plots denote logarithm of frequency.

boundary arcs of the impedance plot, and a part of the electrode arc, allowing a graphical estimation of r_{gi} and r_{gb}.

4. Results

4.1. Electrical measurements

Complex resistivity plots, obtained for samples of CaO–PSZ and CaO + MgO–PSZ after ageing for various times, are shown in Figs. 3 and 4. In all cases the plots consist of three arcs, corresponding to grain interior, grain boundary and electrode interface. It can be seen that there are significant changes in the a.c. plots with ageing for both materials. The chord lengths r_{gi} and r_{gb} were estimated graphically. The electrode arc was not investigated because it is not a true property of PSZ but depends on electrode preparation. Capacitance values c_{gi} and c_{gb}, corrected for sample geometry, were obtained from plots of ρ' against $\log f$. The variations of these quantities are plotted against ageing time at 1400° C for CaO–PSZ in Fig. 5 and for CaO + MgO–PSZ in Fig. 6. The values for as-fired samples are also indicated.

4.2. X-ray diffraction and electron microscopy

X-ray diffraction demonstrated that the t → m transformation in the CaO–PSZ samples occurred relatively sharply after approximately 20 hours ageing, with essentially 100% conversion to m after 30 h. The proportion of the m phase calculated from the m and c peak intensities, using Equation 3, was found to be 0.3. TEM examination confirmed this value; a dark field micrograph showing the t phase distribution in a 10 h sample appears in Fig. 7. The t particles are irregular ellipsoids and of a similar aspect ratio to those observed in aged MgO–PSZ, where $a/b \simeq 2.5$ and $b/c \simeq 2$ [20].

In the ternary composition the X-ray results demonstrated that the transformation commenced at approximately 10 h ageing but was still incom-

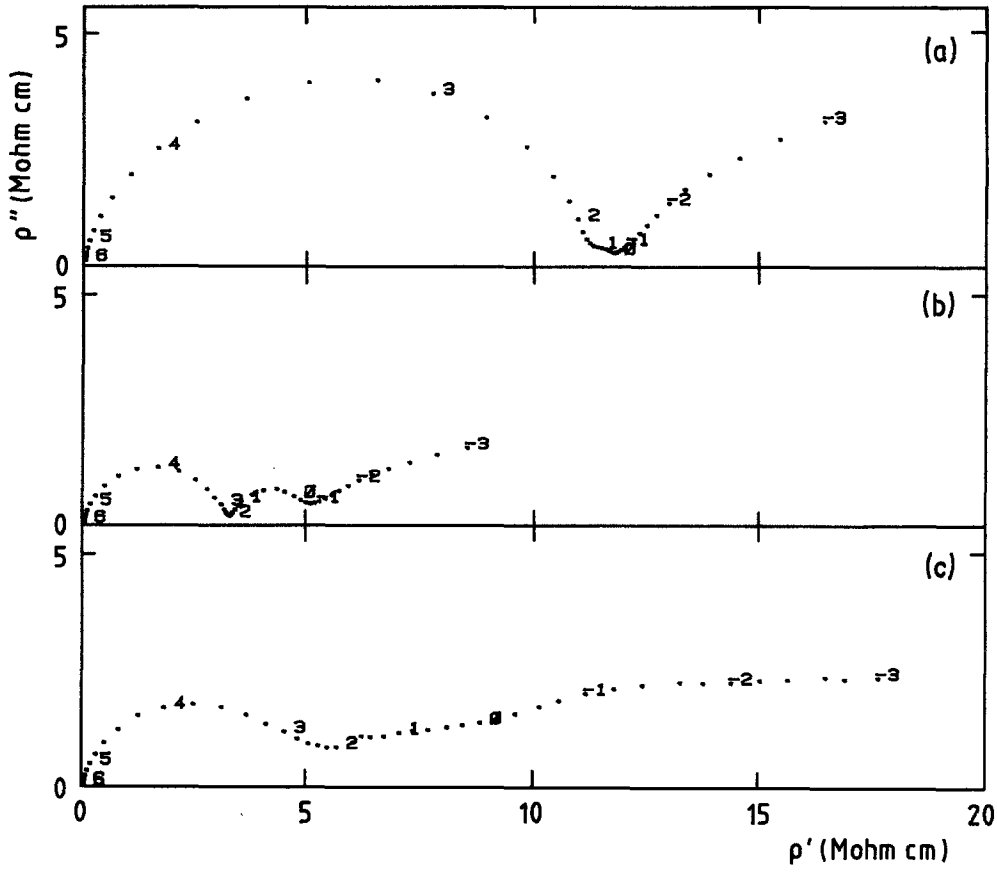

Figure 4 Complex resistivity plots obtained at 300° C for CaO + MgO–PSZ samples: (a) as-fired, (b) aged 10 h, (c) aged 60 h. Numbers on plots denote logarithm of frequency.

plete following 40 h ageing. TEM examination indicated that this was due to a much broader t particle size distribution relative to CaO–PSZ. A further difference was noted in the t phase morphology, which was more elongated and irregular than for CaO–PSZ.

The phase and microstructural evolution of both compositions was similar in the early stages of ageing. The as-fired microstructures were two-phase and consisted of a dispersion of very fine t precipitates in c matrix (t particle size is typically 3 to 5 nm). Ageing resulted in an initial increase in the volume fraction of the t phase, accompanied by steady particle growth.

5. Discussion

5.1. Ageing behaviour of r_{gi}, c_{gi}, r_{gb} and c_{gb}

In the ageing plots of Figs. 5 and 6, the resistivity of the grain interiors, r_{gi} shows three well-defined stages of behaviour. Over the first few minutes there is a sharp fall (Stage I), after which the value of r_{gi} stays approximately constant (Stage II), until finally there is a rise and a levelling off (Stage III). In the binary system the latter occurs after 20 h, coinciding with the t → m transformation, while in the ternary system this process is less well defined and there is a greater degree of scatter in the results. The corresponding capacitance, c_{gi}, also undergoes change in the initial stage of ageing, but the results do not show a clear trend and cannot be easily interpreted.

The grain boundary component of resistivity, r_{gb}, shows a rise with ageing in the binary system, but does not vary as widely as r_{gi}. It is known that r_{gb} is not the actual resistivity of the grain boundary phase [15] – this is normally much higher – but is determined by the geometry of the grain boundary imperfections at which intergranular contact is established. The increase in r_{gb} is therefore related to growth of large monoclinic and other grain boundary phases [14] resulting in closure of these imperfections. By contrast, there is no systematic increase in r_{gb} in the ternary system. In the binary system the grain

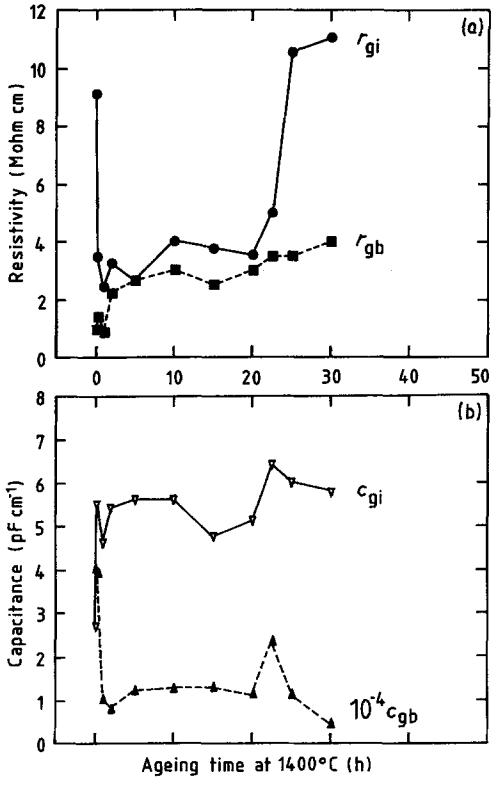

Figure 5 Variation with ageing of quantities extracted from complex impedance plots, for CaO–PSZ: (a) resistivities of grain interior, r_{gi}, and grain boundary, r_{gb}; (b) capacitances of grain interior, c_{gi}, and grain boundary, c_{gb}, corrected for sample shape.

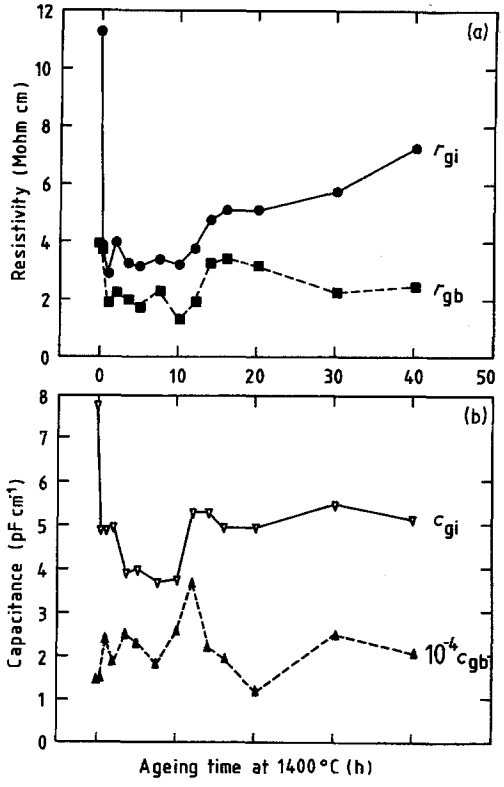

Figure 6 Variation with ageing of quantities extracted from complex impedance plots, for CaO + MgO–PSZ: (a) resistivities of grain interior, r_{gi}, and grain boundary, r_{gb}; (b) capacitances of grain interior, c_{gi}, and grain boundary, c_{gb}, corrected for sample shape.

boundary capacitance, c_{gb}, decreases with ageing, particularly in the early stages. As c_{gb} is inversely proportional to grain boundary thickness, this result also suggests growth of the grain boundary phases. Once again this effect is not found in the ternary system.

In the remaining sections the evolution of the quantity r_{gi} is considered in terms of the electrical properties of the constituent phases of PSZ and the microstructural changes occurring on ageing.

5.2. Relationship between r_{gi} and microstructure throughout ageing

To determine the sensitivity of the quantity r_{gi} to microstructural variables, Equation 2 was used to calculate the d.c. conductivity σ_0 of a dispersion while varying input parameters: x_2, a/b, and b/c. Using imput parameters as deduced in Section 5.3, σ_0 was found to be:

1. Insensitive to particle size, since this quantity does not enter into Equation 2.

2. Relatively insensitive to particle shape; a 30% increase in σ_0 required a 300% increase in axial ratio b/c.

3. Sensitive to volume fraction x_2; a corresponding 30% increase in σ_0 required a 37% increase in x_2.

Before the commencement of the 1400° C ageing the as-fired samples have a non-equilibrium

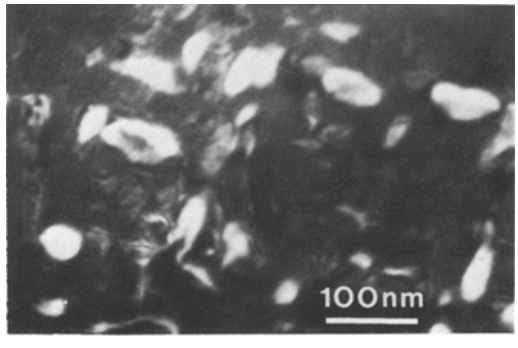

Figure 7 Dark field transmission electron micrograph showing tetragonal precipitate size and distribution in CaO–PSZ aged for 15 h (1000 kV).

TABLE I Values of grain interior conductivity measured on three commercial samples of CaO–FSZ at 300° C [30]

Sample No.	Manufacturer	Composition (mol% CaO)	$\sigma_c(\Omega^{-1}\,cm^{-1})$	Impurities
Iupac 2	Degussit	12.8	8.7×10^{-8}	Si, Al
Iupac 3	Nuclear Research	15.0	9.1×10^{-8}	Si, Al
Iupac 4	Nippon Kagaku	15.0	2.0×10^{-7}	Si, Al, Mg

structure, quenched-in by the relatively fast furnace cool. Inspection of the ZrO_2/CaO phase diagram [25] shows that this implies lower solute content in both the c and t phases. In the early part of ageing, diffusion results in solute enrichment and an increase in volume fraction and size of the tetragonal precipitates. Since σ_0 is insensitive to size and only slightly sensitive to shape of the precipitates, the fall in r_{gi} during Stage I cannot be explained by particle growth or morphological changes. Compositional changes, however, may be responsible, since in the process of equilibration both c and t become enriched in solute, and the conductivity of c is known to increase with stabilizer content [26]. The increase in volume fraction of t phase provides a further possible explanation if this phase has a higher conductivity than the cubic matrix. This premise is surprising in view of the inference from other studies that $\sigma_c > \sigma_t$ [27, 28]. Nevertheless the quantitative analysis of the Stage II → III transition, to be presented in the next section, supports the suggestion that $\sigma_t > \sigma_c$.

Stage II may be regarded simply as a period of coarsening at constant volume fraction of t phase. The approximate constancy of r_{gi} during this stage is consistent with this interpretation since σ_0 should be invariant with the precipitate particle size. The large increase accompanying the transition from Stage II to Stage III (Fig. 5a) coincides with the t → m transformation of the precipitates, as shown by X-ray diffraction and TEM, and demonstrates that $\sigma_t > \sigma_m$.* Since the transformation occurs at constant composition, σ_c must also remain constant. This constraint proves crucial in establishing the relative magnitudes of σ_t, σ_c and σ_m, as shown in the following section.

5.3. Determination of conductivities of individual phases

If the total d.c. conductivity of the dispersion σ_0 and matrix σ_1 are both known, Equation 2 may be solved for the conductivity of the dispersed phase σ_2, given an estimate of the volume fraction x_2 and the form factors. In the case of spherical particles there is an explicit solution [19], but in general a numerical solution must be obtained. If the value of σ_0 is chosen to be equal to $1/r_{gi}$ for Stages II and III, solution of Equation 2 for σ_2 will result in σ_t and σ_m respectively. These solutions should be both obtainable for the same value of σ_1, as this should be constant throughout the transition and equal to σ_c.

For PSZ the matrix conductivity may be estimated from measurements made on fully stabilized samples (FSZ) of commercial CaO–ZrO_2 (Table I); since corresponding measurements do not exist for fully stabilized CaO + MgO–ZrO_2 the following treatment is restricted to the binary system.

The values of σ_0 determined experimentally (Fig. 5a) were $2.9 \times 10^{-7}\,\Omega^{-1}\,cm^{-1}$ for Stage II and $9.1 \times 10^{-8}\,\Omega^{-1}\,cm^{-1}$ for Stage III. The volume fraction, x_2 was taken as 0.3. Although it was difficult to measure accurately the shapes of the particles from electron micrographs (Fig. 7), we estimated the axial ratios a/b and b/c to be close to 2, giving form factors of $\phi_1 = 7.9$, $\phi_2 = 2.5$ and $\phi_3 = 0.66$. Equation 2 was solved numerically using Newton's method for values of σ_c ranging from 10^{-8} to $3 \times 10^{-7}\,\Omega^{-1}\,cm^{-1}$, reflecting uncertainty in the values of σ_c listed in Table I. The results appear in Fig. 8, where σ_c, σ_t and σ_m are plotted against σ_c. It can be seen that only over a limited range of σ_c do both σ_t and σ_m have finite positive values; at lower values of σ_c, σ_t tends to infinity, while at higher values of σ_c, σ_m tends through zero to negative values. For the experimentally determined values of input parameters, σ_c lies between 1.05×10^{-7} and $1.55 \times 10^{-7}\,\Omega^{-1}\,cm^{-1}$. It is important to note that the σ_c values measured for CaO–FSZ (Table I)

*It should be noted that the ionic conductivity of some compounds may be enhanced by the incorporation of fine non-conducting particles, e.g., in LiI doped with Al_2O_3 [29]; this effect seems to be due to the formation of conductive, defect-rich interfaces. There would be no need to postulate that the t phase has a high conductivity if this mechanism were responsible for conduction in PSZ. However, in such a case, m particle interfaces should also be similarly conductive and thus it would not be possible to account for the increase in r_{gi} during the transition from Stage II to Stage III.

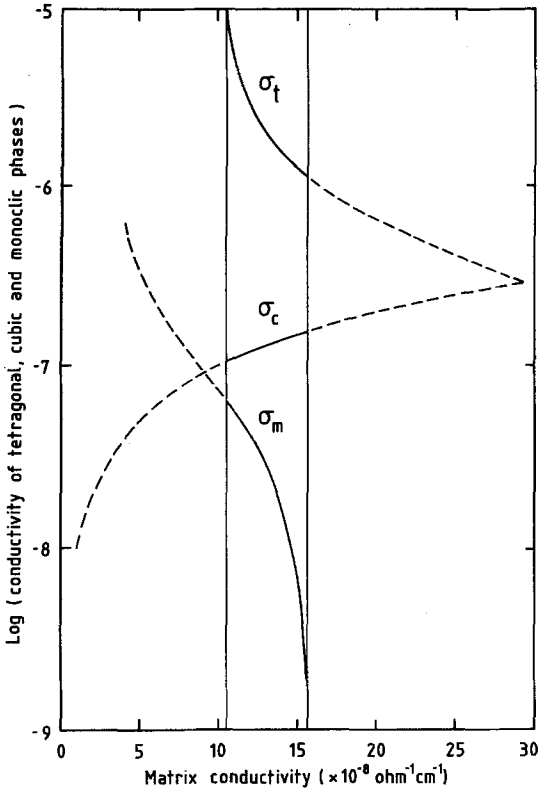

Figure 8 Individual conductivities σ_c, σ_t and σ_m plotted against σ_c. Dispersed phase conductivities σ_t and σ_m are numerical solutions of Equation 2 for assumed values of σ_c. Over the range of σ_c for which solutions exist (solid lines) the relationship $\sigma_t > \sigma_c > \sigma_m$ is found to be valid.

bracket this range. Within the range of validity there are combinations of conductivities σ_c, σ_t, σ_m, which correctly reproduce the values of σ_0 for Stage II and for Stage III. This analysis demonstrates that at 300° C the conductivity relationship is $\sigma_t > \sigma_c > \sigma_m$ even allowing for some error in the input data. This result provides the justification needed for the explanation of the Stage I fall in r_{gi}, presented earlier.

5.4. Applicability of the a.c. model to two-phase dispersions

In all three regions of ageing only one clearly discernible r_{gi} arc was observed in the complex resistivity plane. This is apparently in conflict with Equation 2 and Fig. 2b which predict four R–C elements for the response of the grain interiors alone. This discrepancy was investigated by calculating the theoretical complex resistivity plot for a two-phase dispersion, using Equation 2 for a range of frequencies. As input parameters, σ_c was taken as $1.3 \times 10^{-7}\ \Omega^{-1}\ cm^{-1}$, (close to mid-point of the range over which Equation 2 is soluble) and σ_t and σ_m were read off Fig. 8 for this value of σ_c as 1.9×10^{-6} and $2.7 \times 10^{-8}\ \Omega^{-1}\ cm^{-1}$ respectively. The dielectric constants ϵ_c, ϵ_t, ϵ_m, were taken as equal to the overall dielectric constant of the samples, namely $3.3 \times 10^{-12}\ pF\ cm^{-1}$, as determined from complex modulus plots [31]. Values

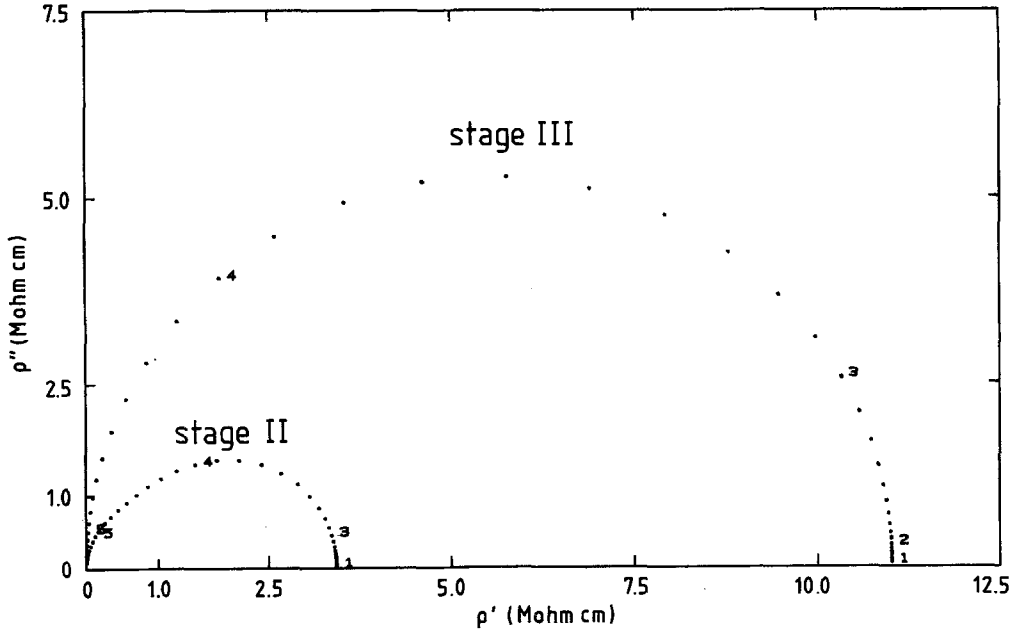

Figure 9 Complex resistivity plots calculated according to Equation 2 for matrix and dispersed phase conductivities corresponding to: (a) Stage II: $\sigma_c = 1.3 \times 10^{-7}$, $\sigma_t = 1.9 \times 10^{-6}\ \Omega^{-1}\ cm^{-1}$; (b) Stage III: $\sigma_c = 1.3 \times 10^{-7}$, $\sigma_m = 2.7 \times 10^{-8}\ \Omega^{-1}\ cm^{-1}$.

of the volume fraction and form factors were those used in Section 5.3.

Fig. 9 shows the calculated complex resistivity plots corresponding to Stages II and III. Although neither of the calculated plots is a perfect semicircle – reflecting the existence of more than one relaxation – the individual relaxations are not clearly resolvable. This is the situation found experimentally (see Fig. 3).

6. Conclusions

1. The grain interior and grain boundary component resistivities of CaO–PSZ and CaO + MgO–PSZ change appreciably during ageing in the two-phase c + t region. The r_{gi} component exhibits three well-defined stages, attributed to equilibration (I), coarsening (II), and t → m transformation (III).

2. Fricke's model for the a.c. conductivity of a two-phase dispersion is applied in conjunction with TEM and X-ray studies to explain the variations in r_{gi}.

3. This approach permits the extraction of the individual conductivities of the cubic, tetragonal and monoclinic phases and indicates that $\sigma_t > \sigma_c > \sigma_m$.

4. The implication of this finding is that the presence of a high volume fraction of tetragonal phase should be beneficial in high conductivity zirconia ceramics.

Acknowledgement

The financial assistance of Anderman & Ryder Ltd and the Science and Engineering Research Council is gratefully acknowledged.

References

1. R. C. GARVIE, R. H. J. HANNINK and R. T. PASCOE, *Nature* **258** (1975) 703.
2. R. V. WILHELM and D. S. EDDY, *Ceram. Bull.* **56** (1977) 509.
3. B. C. H. STEELE, J. DRENNAN, R. K. SLOTWINSKI, N. BONANOS and E. P. BUTLER, in "Science and Technology of Zirconia", Advances in Ceramics, Vol. 3, edited by A. H. Heuer and L. W. Hobbs (The American Ceramic Society, Columbus, Ohio, 1981) p. 286.
4. R. E. CARTER and W. L. ROTH, in "EMF Measurements in High Temperature Systems", edited by C. B. Alcock (IMM, London, 1968) p. 125.
5. T. H. ETSELL and S. N. FLENGAS, *Chem. Rev.* **70** (1970) 339.
6. R. T. PASCOE, R. R. HUGHAN and R. C. GARVIE, *Sci. Sintering* **11** (1979) 185.
7. R. H. J. HANNINK, K. A. JOHNSTON, R. T. PASCOE and R. C. GARVIE, in "Science and Technology of Zirconia", Advances in Ceramics, Vol. 3, edited by A. H. Heuer and L. W. Hobbs (The American Ceramic Society, Columbus, Ohio, 1981) p. 116.
8. R. C. GARVIE, R. H. J. HANNINK and C. URBANI, *Ceramurgia* **6** (1980) 19.
9. R. T. PASCOE, R. H. J. HANNINK and R. C. GARVIE, *Sci. Ceram.* **9** (1977) 447.
10. D. L. PORTER and A. H. HEUER, *J. Amer. Ceram. Soc.* **60** (1977) 183.
11. *Idem, ibid.* **62** (1979) 298.
12. K. KOBAYASHI, H. KUWAJIMA and T. MASAKI, *Solid State Ionics* **3/4** (1981) 489.
13. A. G. EVANS and A. H. HEUER, *J. Amer. Ceram. Soc.* **63** (1980) 241.
14. R. K. SLOTWINSKI, N. BONANOS, B. C. H. STEELE and E. P. BUTLER, in "Engineering with Ceramics", Proceedings of the British Ceramic Society, Vol. 32, edited by R. W. Davidge (The British Ceramic Society, Stoke-on-Trent, 1982) p. 41.
15. J. E. BAUERLE, *J. Phys. Chem. Solids* **30** (1969) 2657.
16. J. M. WIMMER, H. C. GRAHAM and N. M. TALLAN, in "Electrical Conduction in Ceramics and Glasses", edited by N. M. Tallan (Marcel Decker, New York, 1974) Part B, p. 619.
17. R. E. MEREDITH and C. W. TOBIAS, in "Advances in Electrochemistry and Electrochemical Engineering" Vol. 2, edited by C. W. Tobias (Interscience, New York, London, 1962) p. 15.
18. H. FRICKE, *Phys. Rev.* **24** (1924) 575.
19. *Idem., J. Phys. Chem.* **57** (1953) 934.
20. R. J. H. HANNINK, *J. Mater. Sci.* **13** (1978) 2487.
21. J. R. MACDONALD, in "Electrode Processes in Solid State Ionics", edited by M. Kleitz and J. Dupuis (D. Reidel, New York, 1976).
22. J. C. MAXWELL, "A Treatise in Electricity and Magnetism", 2nd edn (Clarendon Press, Oxford, 1881).
23. K. W. WAGNER, *Archiv fur Elektrotechnik* **2** (1914) 371.
24. R. C. GARVIE and P. S. NICHOLSON, *J. Amer. Ceram. Soc.* **55** (1972) 303.
25. V. S. STUBICAN and S. P. RAY, *ibid.* **60** (1977) 534.
26. A. NAKAMURA and J. B. WAGNER, *J. Electrochem. Soc.* **127** (1980) 2325.
27. F. K. MOGHADAM, T. YAMASHITA and D. A. STEVENSON, in "Science and Technology of Zirconia", Advances in Ceramics, Vol. 3, edited by A. H. Heuer and L. W. Hobbs (The American Ceramic Society, Columbus, Ohio, 1981) p. 364.
28. F. K. MOGHADAM and D. A. STEVENSON, *J. Amer. Ceram. Soc.* **65** (1982) 213.
29. C. C. LIANG, *J. Electrochem. Soc.* **120** (1973) 1289.
30. J. DRENNAN *et al.*, to be published.
31. I. M. HODGE, M. D. INGRAM and A. R. WEST, *J. Electroanal. Chem.* **74** (1976) 125.

Received 9 June
and accepted 29 June 1983